Author Manuscript

Author Manuscript

Author Manuscript

Author Manuscript

HHS Public Access

Author manuscript

*J Immunol*. Author manuscript; available in PMC 2024 August 15.

Published in final edited form as:

*J Immunol*. 2023 August 15; 211(4): 563–575. doi:10.4049/jimmunol.2200715.

# Differential effects of glutamine inhibition strategies on anti-tumor CD8 T cells

**Matthew Z. Madden**[*], **Xiang Ye**[*], **Channing Chi**[*], **Emilie L. Fisher**[*], **Melissa M. Wolf**[†], **Gabriel A. Needle**[‡], **Jackie E. Bader**[*], **Andrew R. Patterson**[*], **Bradley I. Reinfeld**[†], **Madelyn D. Landis**[†], **Emma S. Hathaway**[*], **Jason E. Muka**[*], **Richard T. O'Neil**[§], **John Karijolich**[*,‡], **Mary Philip**[†,‡], **Jeffrey C. Rathmell**[*,‡]

[*]Department of Pathology, Microbiology, and Immunology, Vanderbilt University Medical Center, Nashville, TN

[†]Department of Medicine, Vanderbilt University Medical Center, Nashville, TN

[‡]Vanderbilt Center for Immunobiology, Nashville, TN

[§]Department of Veterans Affairs, Ralph H Johnson VA Medical Center and Department of Microbiology and Immunology, Medical University of South Carolina, Charleston, SC

## Abstract

Activated T cells undergo metabolic reprogramming to meet anabolic, differentiation, and functional demands. Glutamine supports many processes in activated T cells, and inhibition of glutamine metabolism alters T cell function in autoimmune disease and cancer. Multiple glutamine-targeting molecules are under investigation, yet the precise mechanisms of glutamine-dependent CD8 T cell differentiation remain unclear. We show that distinct strategies of glutamine inhibition by glutaminase-specific inhibition with small molecule CB-839, pan-glutamine inhibition with 6-diazo-5-oxo-L-norleucine (DON), or by glutamine deprivation (No Q) produce distinct metabolic differentiation trajectories in murine CD8 T cells. T cell activation with CB-839 treatment had a milder effect than DON or No Q treatment. A key difference was that CB-839-treated cells compensated with increased glycolytic metabolism, while DON and No Q-treated cells increased oxidative metabolism. However, all glutamine treatment strategies elevated CD8 T cell dependence on glucose metabolism, and No Q treatment caused adaptation toward reduced glutamine dependence. DON treatment reduced histone modifications and numbers of persisting cells in adoptive transfer studies, but those T cells that remained could expand normally upon secondary antigen encounter. In contrast, No Q-treated cells persisted well yet demonstrated decreased secondary expansion. Consistent with reduced persistence, CD8 T cells activated in the presence of DON had reduced ability to control tumor growth and reduced tumor infiltration in adoptive cell therapy. Overall, each approach to inhibit glutamine metabolism confers distinct effects on CD8 T cells and highlights that targeting the same pathway in different ways can elicit opposing metabolic and functional outcomes.

Address correspondence to Dr. Jeffrey C. Rathmell; phone (615) 936-1764; jeff.rathmell@vumc.org; Department of Pathology, Microbiology, and Immunology, Vanderbilt University, C3322 MCN, 1161 21st Avenue South, Nashville, TN 37232.

Author Manuscript Author Manuscript Author Manuscript Author Manuscript

## Introduction

Glutamine-targeting therapeutics are of interest in oncology to target both cancer cell metabolism and enhance immunity (1, 2). Different inhibitors of glutamine metabolism are in development (3), including glutaminase (GLS)-specific inhibitor CB-839 (telaglenastat) and pan-glutamine inhibitor 6-diazo-5-oxo-L-norleucine (DON), a glutamine-mimetic which irreversibly and competitively inhibits multiple glutamine-utilizing enzymes including GLS (4). In the context of the tumor microenvironment, glutamine-targeting drugs affect not only the metabolism of cancer cells but also immune cells. Their effect on anti-tumor CD8 T cell function is of particular interest to evaluate overall consequences of systemic glutamine inhibition and for their application during the *ex vivo* production of tumor-specific adoptive cell therapies (ACT) such as chimeric antigen receptor (CAR) and TCR-transgenic T cells (5).

Previous studies have shown that glutamine promotes effector T cell function. T cell activation increases glutamine uptake and induces a transcriptional program that promotes glutaminolysis (6). T cells activated in the absence of glutamine show decreased cell blasting and proliferation, although TCR signaling and activation marker upregulation remain intact (7). In CD4 T cells, *in vitro* differentiation in glutamine-depleted media promoted iTreg differentiation dependent on α-ketoglutarate downstream of glutamine (8). Correspondingly, inhibition of glutamic-oxaloacetic transaminase 1 (GOT1) reduced α-ketoglutarate to promote iTreg over Th17 differentiation (9). Deficiency of glutamine transporter ASCT2 (*Slc1a5*) decreased Th1 and Th17 CD4 T cell differentiation *in vitro* and attenuated CD4 T cell-dependent inflammation *in vivo* but did not alter iTreg (10). GLS inhibition or genetic deficiency of *Gls* decreased Th17 differentiation *in vitro*, attenuated inflammation *in vivo* (11–13), but promoted Th1 and cytotoxic differentiation (14). Diverse mechanisms have been proposed for the differential effects of glutamine perturbations. The regulation of reactive oxygen species through glutathione production supported GLS-dependent Th17 differentiation (14). Altered epigenetic marks secondary to reduced availability of α-ketoglutarate necessary for epigenetic modifying enzyme function also affected Th17 and Th1 fates (14, 15). Glutamine efflux promotes the cotransport of branched chain amino acids. T cells with genetic deficiency of large neutral amino acid transporter LAT1 (*Slc7a5*) demonstrated a marked failure to proliferate and gain effector function partially dependent on the presence of glutamine for cotransport (16).

Precise roles for glutamine in CD8 T cell differentiation and function are unclear. There is substantial evidence that blocking anabolic pathways in tumor-specific CD8 T cells during *in vitro* expansion for ACT promotes a stem-like phenotype that enhances anti-tumor activity *in vivo* (5). Tumor growth was better controlled when tumor specific CD8 T cells were activated in glutamine-depleted media, with pan-glutamine inhibition by DON, or with inhibitors of the conversion of glutamate to α-ketoglutarate. Cells activated in depleted glutamine conditions also demonstrated enhanced oxidative and glycolytic metabolism, enhanced cytotoxicity, and increased markers of stem-like differentiation (17). Correspondingly, GLS inhibition with small molecule CB-839 enhanced CD8 T cell effector differentiation and promoted CAR T cell persistence *in vivo* and effector function *in vitro* (14). CB-839 treatment *in vivo* also enhanced adoptive cell therapy and immune checkpoint

Author Manuscript Author Manuscript Author Manuscript Author Manuscript

blockade therapies (18). *In vivo* treatment with a DON derivative promoted anti-tumor CD8 T cell activity associated with enhanced anabolic flux. Strikingly, DON treatment of cancer cells had the reverse effect, causing reduced growth and upregulated catabolic metabolism (19). DON has also been shown to enhance the efficacy of cancer vaccines and anti-tumor myeloid cell activity (20, 21). However, it is not clear that targeting glutamine metabolism is beneficial for CD8 T cell activity in all contexts, as CB-839 decreased CD8 activation in other preclinical models (22). Both CB-839 and DON are being developed as treatments for oncology patients, and different nutrient-centric strategies of producing better ACT are being investigated (4, 5, 23).

Here we hypothesized that because each glutamine inhibition strategy targets different enzymes, they may differ in their effect on CD8 T cell fate and anti-tumor activity. We compared CD8 T cell differentiation and function between cells activated with control conditions, GLS-specific inhibition by CB-839, pan-glutamine inhibition by DON, or glutamine-depleted conditions (No Q). We found that GLS-specific inhibition had a smaller effect on overall CD8 T cell differentiation compared to DON and No Q treatments. DON treatment reduced the number of persisting CD8 T cells after adoptive transfer and impaired control of tumor growth. In contrast, No Q-treated CD8 T cells had no change in persistence but had impaired secondary recall response to antigen. These differences were associated with distinct metabolic differentiation trajectories that were mirrored by transcriptomic and epigenetic changes. Ultimately, our results demonstrate that strategies targeting glutamine metabolism during CD8 T cell activation can impair cell expansion and differentiation. The timing and mode of glutamine antagonism, therefore, will be critical for the *in vitro* production of ACTs and should be considered for systemic anti-tumor immunity.

## Materials and methods

### Mice

Thy1.1 (000406) and OT-I transgenic (003831) mice were obtained from the Jackson Laboratory. The F1 generation of Thy1.1 homozygous crossed to OT-I homozygous mice were used for OT-I *in vitro* and adoptive transfer experiments. OT-I mice homozygous for CD45.1 were also used for some tumor growth, survival, and tumor-infiltrating OT-I profiling. CD4-Cre $Gls^{fl/fl}$ mice were generated as previously described (14). Wild-type CD4-Cre negative $Gls^{fl/fl}$ mice were compared to knockout CD4-Cre positive $Gls^{fl/fl}$ littermates. Both male and female mice were utilized in experiments. All mouse procedures were performed under Institutional Animal Care and Use Committee (IACUC)-approved protocols from Vanderbilt University Medical Center and conformed to all relevant regulatory standards. Mice were housed in ventilated cages with at most 5 animals per cage and provided ad libitum food and water. Mice were on 12 hour light/dark cycles which coincided with daylight in Nashville, TN. The mouse housing facility was maintained at 68–76°F and 30–70% humidity. For injectable tumor models, 8–20 week old male and female mice were used. Mice were euthanized (survival endpoint) for 2cm tumor dimension, ulceration, or weight loss >10%. Tumor calipering and mouse weighing was performed every other day blinded to treatment group and previous measurements.

Author Manuscript Author Manuscript Author Manuscript Author Manuscript

## Cancer cell lines

The MC38 cell line was provided by Barbara Fingleton (Vanderbilt University Medical Center). The MC38-OVA cell line was generated by co-transfecting 5 million MC38 cells with 5μg sleeping beauty transposon plasmid encoding a murine codon optimized SIINFEKL peptide driven by a CAG promoter (24) along with 5μg of a plasmid driving expression of sleeping beauty transposase (https://www.addgene.org/34879/) by electroporation using a NEON nucleofector by the manufacturer recommended protocol. These cells were plated as single cells by limiting dilution into a 96-well plate to generate clonal cell lines. These lines were screened for OVA expression by flow cytometry using an antibody specific for SIINFEKL presented in the context of H2-Kb (25-D1.16, eBioscience eBio25-D1.16) and positive clonal lines were transplanted subcutaneously into male C57BL6 mice to determine tumorigenicity. This line was derived from a clone that formed tumors in >75% of mice. Cells were grown in DMEM supplemented with 10% FBS. Cells were trypsinized, washed twice in PBS, and $1\times10^6$ cells were injected subcutaneously in 100–200μL of PBS on mouse flanks. Subcutaneous tumors grew for 14–24 days prior to analysis by flow cytometry.

## T cell culture and adoptive transfer

OT-I mouse splenocytes were ACK-lysed and resuspended to 2 million splenocytes/mL in complete RPMI media supplemented with 10% FBS, pen/strep, HEPES, glutamine, and β-mercaptoethanol, or in complete RPMI without glutamine (No Q). OT-I cells were activated with 100 IU/mL recombinant human IL-2 (rhIL-2, NCI) and 10ng/mL SIINFEKL peptide (Sigma-Aldrich S7951). CB-839 (MedChemExpress HY-12248) or equal volume DMSO vehicle and DON (Sigma-Aldrich D2131) or equal volume PBS vehicle were added to a final concentration of 1μM as has been performed previously (14, 17, 19). 2-deoxyglucose (Cayman Chemical 14325) or equal volume water vehicle was added to a final concentration of 1mM. Twenty-four hours later, CD8 T cells were isolated via negative selection using the CD8 isolation kit (Miltenyi 130-095-236) according to manufacturer instructions to remove antigen presenting cells prior to T cell proliferation and T cells were resuspended at 200,000 cells/mL in media plus drug and 100 IU/mL rhIL-2. For bulk processing of cells prior to 24hr for extracellular flux analysis and RNAseq, OT-I cells were isolated with a CD8 isolation kit and purity was checked by flow cytometry. For adoptive transfer experiments, 500,000 48hr-activated OT-I cells were transferred into mice via retroorbital injection. For transfer of persisting memory-like cells into a naïve recipient, Thy1.1 positive selection beads (Miltenyi 130-121-273) were used on splenocytes, purity was measured by flow cytometry, and 400 OT-I cells with carrier splenocytes were transferred into recipient mice before *Listeria monocytogenes* expressing OVA (Lm-OVA) infection the next day. Peripheral blood was collected from mice 3 days after adoptive transfer by cheek bleed using lancets (5mm, Goldernrod) and heparinized Natelson blood collecting tubes (Fisher 03-668-10). 25μL whole blood was washed twice with 200μL PBS, treated for 5min with 200μL ACK lysis solution, and stained for flow cytometry analysis. For extended culture of 48hr-activated OT-I cells, OT-I cells were resuspended at 250,000 cells/mL in 10ng/mL recombinant mouse IL-7 (R&D Systems 407-ML), 100 IU/mL rhIL-2, or 100 IU/mL rhIL-2 in plates with bottoms coated with PBS with 5μg/mL αCD3/28 (clone145-2C11, Invitrogen 16-0031-86) (clone 37.51, Invitrogen 16-0281-86) for 3 additional days, with

Author Manuscript Author Manuscript Author Manuscript Author Manuscript

media replaced 48hr after plating. Polyclonal CD4-Cre *Gls*$^{fl/fl}$ splenic CD8 T cells were isolated using the CD8 isolation kit and were activated *in vitro* in rhIL-2 for 24hr with αCD3/28 beads (Thermo Scientific 11456D) according to manufacturer's instructions and cultured for another 48hr in rhIL-2.

### Lm-OVA infection

*Listeria monocytogenes* expressing OVA (Lm-OVA) was generated by Aduro Biotech and provided by the Mary Philip lab (25). Lm-OVA was stored at −80°C. Mice were injected intraperitoneally with $1\times10^7$ CFU.

### Tissue processing to single cells

Spleens and livers were dissociated with a syringe, passed through a 70μm filter, and ACK-lysed. Tumors were chopped, mechanically dissociated on the Miltenyi gentleMACS Octo Dissociator with Heaters (setting implant tumor one) and digested in 435 U/mL DNase I (Sigma-Aldrich D5025) and 218 U/mL collagenase (Sigma-Aldrich C2674) at 37 °C for 30 min. Then, tumors were passed through a 70μm filter and ACK-lysed. Gonadal adipose tissue was dissected from mice and minced with scissors in FACS buffer. To isolate the stromal vascular fraction, minced adipose tissue was incubated for 30min with rocking in FACS buffer supplemented with 4mg/mL Type II collagenase (Worthington LS00418) and 0.25mg/mL DNase 1, passed through a 100μm filter, ACK-lysed, and filtered again prior to analysis.

### Flow cytometry

Single cell suspensions were incubated in $F_c$ block (1:50, BD 553142) for 10min at room temp, stained for surface markers for 15min at room temp, washed with FACS buffer (PBS +2% FBS) once, and resuspended in FACS buffer for analysis on a Miltenyi MACSQuant Analyzer 10 or 16. For intracellular staining, the eBioscience™ Foxp3/ transcription factor staining buffer kit (Fisher 00-5523-00) was used. For intracellular cytokine staining, single cell suspensions were incubated for 4hr at 37°C 5% $CO_2$ in supplemented RPMI with PMA (50ng/mL, Sigma Aldrich P8139-1MG), ionomycin (750ng/mL, Sigma Aldrich I0634-1MG), and GolgiPlug (1:1000, BD 555029), and processed using the BD Cytofix/Cytoperm™ Fixation and Permeabilization Solution (ThermoFisher BDB554722). Surface staining was performed as described above, cells were fix/permed for 20min at 4°C, and then stained for intracellular markers for at least 30min at 4°C. Staining occurred in 50μL total volume. Ghost Dye Red 780 viability dye (1:4000, Cell Signaling 18452S) was used identically to surface antibodies. The antibodies used were: CD45 BV510 (1:1600, 30-F11, Biolegend 103138), B220 e450 (1:400, RA3-6B2, ThermoFisher 48-0452-82), CD11b e450 (1:1600, M1/70, ThermoFisher 48-0112-82), CD11b FITC (1:1600, M1/70, Biolegend 101206), CD8a AF488 (1:1600, 53-6.7, Biolegend 100723), CD8a e450 (1:600, 53-6.7, ThermoFisher 48-0081-82), CD8a BV510 (1:600, 53-6.7, BD 563068), CD8a APC (1:200, 53.6-7, BD 17-0081-82), Ly6C FITC (1:4000, HK1.4, Biolegend 128006), CD11c PE (1:1000, N418, BioLegend 117308), FOXP3 PE (1:125, FJK-16s, ThermoFisher 12-5773-82), pS6 Ser235/236 PE (1:100, D57.2.2E, Cell Signaling 5316S), CD4 PerCP-Cy5.5 (1:600, RM4-5, BioLegend 100540), Ly6G PerCP-Cy5.5 (1:800, 1A8, BioLegend 127616), F4/80 PE-Cy7 (1:800, BM8, BioLegend

Author Manuscript Author Manuscript Author Manuscript Author Manuscript

123114), NKp46 PE-Cy7 (1:200, 29A1.4, BioLegend 137618), CD3 PE-Cy7 (1:200, 17A2, BioLegend 100220), CD3 FITC (1:200, 17A2, BioLegend 100204), CD3 APC (1:200 17A2, BioLegend 100236), CD206 APC (1:500, C068C2, BioLegend 141708), Thy1.1 PerCP-Cy5.5 (1:2000, HIS51, ThermoFisher 45-0900-82), Thy1.1 FITC (1:2000, HIS51, ThermoFisher 11-0900-85), PD-1 PE (1:100, 29F-1A12, BioLegend 135206), TIM3 APC (1:100, RMT3-23, BioLegend 119706), IFNγ APC (1:250, XMG1.2, BioLegend 505810), CD25 e450 (1:500, PD61.5, ThermoFisher 48-0251-82), CD44 PE-Cy7 (1:1000, IM7, BioLegend 103030), CD62L APC (1:200, MEL-14, ThermoFisher 17-0621-82), CD69 FITC (1:200, H1.2F3, BioLegend), TCF1 AF647 (1:200, C64D9, Cell Signaling), TBET PE-Cy7 (1:100, eBio4B10, eBioscience 25-5825-82), EOMES PE (1:100, Dan11mag, eBioscience 12-4875-82), Perforin APC (1:100, eBioOMAK-D, eBioscience 17939280), Granzyme B PE (1:100, NGZB, eBioscience 12-8898-80), IL-2 PE (1:100, BD 554428), TNFα PE-Cy7 (1:200, MP6-XT22, BioLegend 506324), CD45.1 BV510 (1:100, A20, BioLegend 110735), and CD45.2 PerCP-Cy5.5 (1:100, 104, BioLegend 109828). The NIH Tetramer Core Facility provided the SIINFEKL PE tetramer (1:1000). CellTrace Violet (CTV) (Thermo Fisher Scientific, C34557) was used at 1:1000 for cell proliferation assays. Mitochondrial mass was measured with 200nM MitoTracker Green FM (Invitrogen M7514) and mitochondrial membrane potential was measured with 150nM TMRE (Lifetech T-669) staining for 30min at 37°C 5% $CO_2$ in complete media. Flow cytometry data were analyzed using FlowJo v10.7.1.

## Extracellular flux assay

T cells were plated at 150,000 live cells/well in technical quadruplicate on a Cell-Tak-coated plate (Corning 354240) in Agilent Seahorse RPMI 1640 supplemented with 10mM glucose, 1mM sodium pyruvate, and 2mM glutamine unless otherwise indicated. Cells were analyzed on a Seahorse XFe 96 bioanalyzer using the Mitostress assay (Agilent 103015-100) with 1μM oligomycin, 2μM FCCP, and 0.5μM rotenone/antimycin A. Data were analyzed in Agilent Wave software version 2.6.

## Proton NMR metabolite analysis

Conditioned culture media was collected at the 48hr timepoint after refreshing media and resuspending to 200,000 cells/mL at 24hr. Media was processed as previously reported (26). Briefly, 50μL $D_2O$ and 50μL of 0.75% sodium 3-trimethylsilyl-2,2,3,3-tetradeuteropropionate (TSP) in $D_2O$ was added to 500 μL media and transferred to 5mm NMR tubes (Wilmad-LabGlass, Kingsport, TN). $^1$H-MRS spectra were acquired on an Avance III 600 MHz spectrometer equipped with a Triple Resonance CryoProbe (TCI) (Bruker) at 298°K with 7500-Hz spectral width, 32,768 time domain points, 32 scans (supernatant), and a relaxation delay of 2.7s. The water resonance was suppressed by a gated irradiation centered on the water frequency. The spectra were phased, baseline corrected, and referenced to TSP using Chenomx NMR Suite. Spectral assignments were based on literature values.

## RNA-sequencing

RNA was extracted from isolated T cells using the Quick-RNA™ Microprep Kit (Zymo R1050) according to manufacturer's instructions. DNase I treated RNA were subjected

Author Manuscript Author Manuscript Author Manuscript Author Manuscript

to BioAnalyzer 2100 for quality assessment and samples with RIN > 7.0 were used for mRNA enrichment and cDNA library preparation utilizing stranded library preparations. Sequencing was performed at Paired-End 150 bp on the Illumina NovaSeq 6000 targeting an average of 50M reads per sample. Library preparation and sequencing occurred at the Vanderbilt Technologies for Advanced Genomics (VANTAGE). Raw read quality was assessed using FastQC (v0.11.5). STAR (v2.7.3a) was used to align reads to the mouse genome (GRCm38.primary assembly from gencode). The transcript quantification was done using featureCounts (v2.0.1) using the pair-end mode to count mated reads that both mapped uniquely. Then the differentially expressed genes were called using edgeR (v2.26.5) with Benjamini-Hochberg adjusted p-value < 0.05. Multidimensional scaling analysis (MDS) was done within edgeR. Then the normalized (count per million) and log transformed gene expression matrix was used for KEGG pathway analysis using R package GSVA (v1.40.1) with KEGG gene sets imported from msigdbr (v7.4.1) and then visualized with pheatmap (v1.0.12).

## CUT&RUN

CUT&RUN (27) was performed using a CUT&RUN kit (Cell Signaling, CUT&RUN Assay Kit, Cat#86652) with a magnetic based method. Briefly, 250,000 purified CD8 T cells were harvested by centrifugation (600g, 3 min) and washed twice with kit wash buffer. The cells were resuspended in 100μl wash buffer and mixed with 10μl pre-activated Concanavalin A beads on a rotator for 5min. Then cells were incubated in antibody binding buffer containing either 2.5μl H3K27me3 antibody (Cell Signaling 9733S), 2.5μl H3K27ac antibody (Cell Signaling 8173S), or 5μl IgG control and incubated at 4°C for 2hr on a rotator. Beads were then washed once in digitonin buffer and resuspended in 100 μl digitonin buffer containing 1.5μl pAG-MNase and incubated at 4°C for 1hr on a rotator. After 2 washes with digitonin buffer beads were resuspended in 150μl digitonin buffer and pAG-MNase was activated with the addition of 3μl $CaCl_2$ to a final concentration of 2mM. Beads incubated in an ice/water mix for 30min to finish the digestion, and the reaction was quenched with 150μl stop buffer. Cleaved fragments were liberated into the supernatant by incubating the beads at 37°C for 10min. DNA fragments were extracted from the supernatant and uniquely dual indexed libraries were prepared with KAPA HyperPrep Kits (KK8504). Sequencing was performed at PE 150 on the NovaSeq 6000 targeting an average of 10M reads per sample. Library preparation and sequencing occurred at the Vanderbilt Technologies for Advanced Genomics (VANTAGE). Paired-end fragments were first trimmed with Trimmomatic (v0.39) to remove adapter and low-quality nucleotides and then mapped to the mouse genome GRCm38.p6 using bowtie2 (v2.3.5.1) with options: --local --very-sensitive-local --no-unal --no-mixed --no-discordant --phred33 -k 1 -I 10 -X 700. Then the alignment SAM files were transformed to BAM and BIGWIG files using samtools (v1.9) and deeptools (v3.3.1) for the following data analysis and visualization. MACS2 (v2.2.7.1) was used for calling peaks with options: --broad -p 0.05 -f BAMPE --keep-dup all. Then IDR (v2.0.3) was used to call the reproducible peaks between replicates with FDR < 0.05. Visualization of histone modification signal along certain genomic regions were done by load the respective bigwig files into IGV (v2.12.0).

Author Manuscript Author Manuscript Author Manuscript Author Manuscript

### Quantification, statistical analysis, and data availability

Graphs and statistical tests were generated using GraphPad Prism 9 unless otherwise noted. Sample sizes were chosen based on previous studies. Graphs show mean and SEM unless otherwise stated. Gene expression and Cut&Run data are available at GEO GSE232241 (https://www.ncbi.nlm.nih.gov/geo/query/acc.cgi?acc=GSE232241).

## Results

### T cell-specific *Gls* knockout and responses to acute infection and tumors

We first hypothesized that CD8 T cells deficient for *Gls* would have altered responses to acute infection or tumors. $Gls^{fl/fl}$ CD4-$Cre^{+}$ mice, in which both CD4 and CD8 T cells have genetic knockout of *Gls*, and CD4-$Cre^{-}$ littermate controls were infected with ovalbumin-expressing *Listeria monocytogenes* (Lm-OVA) and antigen-specific CD8 T cells were analyzed by flow cytometry across multiple timepoints. $Tetramer^{+}$ antigen-specific *Gls*-deficient CD8 T cells demonstrated no changes in total cell abundance or phenotype (Figure 1a–d, Supplemental Figure 1a). Similarly, there was no difference in the growth or immune infiltration of MC38 tumors although the total number of splenic CD8 T cells was reduced in *Gls*-deficient mice (Figure 1e–g, Supplemental Figure 1b–c). Splenic CD8 T cells in *Gls*-deficient tumor-bearing mice also demonstrated larger populations of $CD44^{+}$, $PD\text{-}1^{+}$, and IFNγ-producing cells, whereas tumor *Gls*-deficient CD8 T cells expressed more TIM3 and less IFNγ (Figure 1h–n). These phenotypes are consistent with chronic *Gls* deficiency enhancing terminal CD8 differentiation in both lymphoid tissue and tumors (14).

### *In vitro* glutamine treatment alters *in vivo* fate for DON and No Q CD8 T cells

In the absence of a robust phenotype with chronic knockout of *Gls* in CD8 T cells, we hypothesized that inhibition of glutamine metabolism via distinct strategies during initial *in vitro* activation would alter CD8 T cell persistence and function after adoptive transfer. Splenic $Thy1.1^{+}$ OT-I CD8 T cells were activated with cognate peptide and IL-2 under control, GLS-inhibitor CB-839, pan-glutamine inhibitor DON, and No Q media conditions for up to 48hr and activation and proliferation were measured (Figure 2a). By 48hr, DON and No Q reduced proliferation and live cell yields more strongly than CB-839 without affecting cell viability (Figure 2b–d). Flow cytometry analysis demonstrated upregulation of activation marker CD69 at 4hr, increased size and granularity by 24hr, and proliferation after 24hr of culture (Figure 2e). All glutamine inhibition groups had reduced cell size by 24hr, although this was less stark by 48hr after initial rounds of cell division (Supplemental Figure 2). Activation markers CD69, CD44, and CD25 increased as expected during activation, but in No Q conditions CD44 was delayed and CD69 was elevated. CD62L levels increased relatively more by 48hr in CB839 and DON conditions (Supplemental Figure 2). $Gls^{fl/fl}$ CD4-Cre CD8 T cells activated with αCD3/28 beads demonstrated that *Gls* deficiency mimicked the effect of CB-839 and that CB-839 conferred no additional effect on cell proliferation in *Gls* deficient cells (Figure 2f).

After 48hr of activation, OT-I $Thy1.1^{+}$ CD8 T cells were adoptively transferred into $Thy1.2^{+}$ naïve mice and were analyzed 35 days later to assess the persistence of previously activated memory-like cells. DON treatment significantly reduced the number of $Thy1.1^{+}$ OT-I cells

Author Manuscript Author Manuscript Author Manuscript Author Manuscript

in the spleen (Figure 2g). To determine the functionality of the persisting CD8 T cells, 35-day splenic Thy1.1$^+$ cells were purified with magnetic beads and adoptively transferred in equal numbers into new Thy1.2$^+$ hosts. The next day, the recipient mice were infected with Lm-OVA and secondary effector cells were measured 7 days later (Figure 2h). CB-839 and DON-treated OT-I cells expanded similarly to control OT-I, but No Q OT-I cells were less numerous compared to other glutamine inhibition conditions (Figure 2i). These results suggest that glutamine blockade with DON reduced the expansion or persistence of adoptively transferred cells *in vivo* but those cells that persisted maintained the ability to function as memory cells. Conversely, CD8 T cells stimulated without glutamine *in vitro* persisted *in vivo* but had defective secondary responses weeks later.

We hypothesized that differences of *in vivo* fate may be mirrored by differentiation marker changes over the initial 48hr of activation. Transcription factors TCF1, TBET, and EOMES; coinhibitory receptor PD-1; cytolytic molecules perforin and granzyme B; and cytokines IFNγ, TNFα, and IL-2 demonstrated different trajectories of expression and final levels at 48hr (Supplemental Figure 2). Control CD8 cells appeared to express higher levels of each molecule earlier than the different glutamine treatment T cells, however no clear association could be drawn between these markers and *in vivo* persistence or recall function.

## Glutamine treatments alter the transcriptome

We hypothesized that alterations to the global transcriptome could underly differences in glutamine-inhibited T cell fate. We performed transcriptomic profiling (RNAseq) on *in vitro* activated OT-I cells at 0, 4, 24, and 48hr post-activation in control, CB-839, DON, and No Q conditions. Principal component analysis (PCA) revealed that transcriptomic differences depend on time of activation, with the ability to distinguish DON and No Q samples at 24 and 48hr (Figure 3a). Pearson correlation coefficient analysis also demonstrated grouping according to day of activation, with clear demarcation of DON and No Q samples at 24 and 48hr (Supplemental Figure 3a). DON treatment by 48hr appeared to cause greater differences compared to the other treatments. The overall number of differentially expressed genes (DEGs) over time for each treatment was appoximately the same, although more genes changed for DON and No Q in the 24–48hr interval, with a greater number of both upregulated and downregulated genes with DON treatment (Supplemental Figure 3b). The number of DEG for CB-839 was much lower than for DON and No Q, consistent with its tight clustering with control cells by PCA and Pearson correlation coefficient analysis (Supplemental Figure 3c).

KEGG pathway enrichment analysis demonstrated clustering of distinct processes according to treatment (Figure 3b). At 24hr and 48hr after activation, anabolic metabolic pathways such as the tricarboxylic acid cycle, pentose phosphate pathway, branched chain amino acid biosynthesis, and glycolysis (Supplemental Figure 3d) were elevated in control and CB-839 cells at 24hr and 48hr compared to DON and No Q, consistent with increased proliferation and cell cycle progression (highlighted in upper red box). By 48hr, No Q cells also demonstrated higher levels of cell cycle related pathways compared to DON cells (highlighted in upper red box), although they also demonstrated a stronger autophagy signal

Author Manuscript Author Manuscript Author Manuscript Author Manuscript

(highlighted in lower red box). This may be consistent with CD8 T cells in No Q conditions adapting to glutamine deprivation, in contrast to DON treatment.

## Distinct metabolic differentiation trajectories by glutamine treatments

To characterize the metabolism of glutamine-inhibited CD8 T cells, we performed extracellular flux analysis across 0, 4, 24, and 48hr timepoints of differentiation. Basal extracellular acidification rate (ECAR), a proxy for lactate production from glycolysis, and oxygen consumption rate (OCR), a measurement of oxidative metabolism, demonstrated different trajectories of metabolic differentiation according to treatment (Figure 4a–d). By 4hr, all cells demonstrated increased ECAR consistent with activation-induced glycolysis (Figure 4a, inset). Control and CB-839 cells demonstrated relatively higher ECAR, whereas DON and No Q groups demonstrated relatively higher OCR at the 24hr and 48hr timepoints. These results are consistent with control and CB-839 cells utilizing more glycolysis (14). CB-839 treatment decreased the OCR/ECAR ratio compared to control, suggesting that specific GLS inhibition confers an opposite effect compared to pan-glutamine inhibition or glutamine deprivation (Figure 4e). DON and No Q conditions induced greater maximal OCR by 48hr (Figure 4f), consistent with higher mitochondrial mass in those cells (Supplemental Figure 4a). Although CB-839 reduced basal OCR, it retained a similar maximal OCR with a reduced proton leak compared to control T cells, potentially consistent with greater mitochondrial reserve (Supplemental Figure 4b). Mitochondrial membrane potential by itself or normalized to mitochondrial mass also demonstrated the lowest value in CB-839 cells, potentially consistent with “more fit” mitochondria (Supplemental Figure 4c–d) (28). Correspondingly, *Gls* deficiency demonstrated decreased mitochondrial membrane potential (Supplemental Figure 4e). mTORC1 signaling is critical for anabolic metabolism in proliferating cells including activated CD8 T cells. Glutamine inhibition broadly blunted mTORC1 signaling early during activation as indicated by phosphor-S6, but this subsequently rebounded, particularly with CB-839 treatment (Supplementary Figure 4f). Overall, our results suggest that the metabolic differentiation trajectories of CB-839-treated CD8 T cells varies drastically from DON and No Q-treated cells, with greater glycolysis after GLS-specific inhibition and greater oxidative phosphorylation in pan-glutamine inhibition.

We next asked if CB-839 treatment induced a dependency on compensatory glucose uptake. Consistent with their elevated ECAR, CB-839 CD8 T cells secrete more lactate than other glutamine-treated cells (Figure 5a). OT-I CD8 T cells were activated for 48hr in the four different glutamine conditions with or without hexokinase inhibitor 2-deoxyglucose (2DG) to reduce flux through glycolysis during activation. 2DG reduced live cell yield and had a small effect on viability across glutamine treatments (Figure 5b–c). 2DG treatment induced a compensatory increase in OCR ATP production and maximal respiration in control cells which was not achieved by any glutamine treatment cells, despite similar relative reductions in ECAR (Figure 5d–g). The OCR/ECAR ratio increase with 2DG was significantly lower in glutamine treatments compared to control (Figure 5h). Granzyme B and Perforin levels were substantially reduced in all groups with 2DG treatment (Figure 5i). No Q conditions with inhibition of glycolysis by 2DG yielded the most substantial decrease in metabolic function and activation, and cells did not enter G1 phase as indicated by Ki67 positivity (Figure 5j).

Author Manuscript Author Manuscript Author Manuscript Author Manuscript

Overall, these results suggest that all treatments that inhibit glutamine metabolism in CD8 T cells increase dependency on glycolysis.

## Global H3K27 trimethylation and acetylation are decreased by pan-glutamine inhibition

Epigenetic modifications including histone methylation and acetylation enforce T cell differentiation state (29). Metabolites are the substrates for acetylation and methylation, and α-ketoglutarate downstream of glutamine is a demethylase cofactor. We hypothesized that glutamine inhibition strategies may have differential effects on histone modifications. We performed CUT&RUN (27) to profile genomic regions with acetylated H3K27 (H3K27Ac), associated with open chromatin and increased gene transcription, and trimethylated H3K27 ($H3K27me^3$), associated with closed chromatin and decreased gene transcription. At 48hr, global $H3K27me^3$ was decreased in DON-treated CD8 T cells and the transcripts at those sites were relatively increased (Figure 6a). H3K27Ac was also decreased in DON-treated CD8 T cells and associated with decreased transcript levels (Figure 6b), suggesting that epigenetic modifications may be substantially dysregulated in the presence of pan-glutamine inhibition. Notably, No Q treatment demonstrated increased transcript expression of amino acid transporters including *Slc3a2* and *Slc7a5*, with associated increased H3K27Ac signal at those loci (Figure 6c–d). Correspondingly, amino acids including branched-chain amino acids had elevated net uptake in No Q cells (Figure 6e), suggesting that cells activated without glutamine adapt by increasing uptake of other amino acids. To test the dependence of glutamine on CD8 T cell metabolism, we performed extracellular flux assays to measure changes in flux after an acute injection of glutamine. Control, CB-839, and DON-pretreated CD8 T cells all relatively upregulated OCR in the presence of extracellular glutamine consistent with glutamine uptake supporting glutaminolysis and anaplerosis. No Q T cells, however, did not change their OCR/ECAR ratio in response to glutamine, suggesting they had adapted to glutamine deprivation by not utilizing glutamine for ATP production (Figure 6f).

## CD8 T cells activated in DON have impaired control of tumor growth

To determine how distinct glutamine inhibition strategies affect tumor ACT, we injected MC38-OVA tumor-bearing mice with OT-I CD8 T cells activated for 48hr in control, CB-839, DON, or No Q conditions. The dose of OT-I cells was insufficient to eliminate tumors but did slow tumor growth. DON-treated OT-I cells failed to control tumor growth and extend mouse survival as well as control OT-I cells (Figure 7a–b, Supplemental Figure 4g). DON pretreatment also reduced the abundance of OT-I cells in tumors, spleens, adipose tissue, and tumor-draining lymph nodes (Figure 7c–d, Supplemental Figure 4h). Immunophenotying revealed slight differences in tumor-infiltrating OT-I cells, including slightly more elevated coinhibitory receptors after CB-839 pretreatment and higher levels of Ki67 after DON pretreatment (Figure 7e–h), although overall ex vivo production of IFNγ was similar. No Q pretreatment was associated with higher levels of CD62L in splenic OT-I cells (Figure 7i), and No Q OT-I abundance was relatively low in tumors compared to splenic abundance particularly compared to CB-839 pretreatment (Figure 7d), all potentially consistent with reduced initial activation leading to impaired function similar to the reduced secondary recall response above (Figure 2i). We observed that the reduced number of DON pretreated cells was present as early as 3 days post transfer in peripheral blood (Figure 7j).

Author Manuscript Author Manuscript Author Manuscript Author Manuscript

Similarly, DON pretreated cells did not persist as well as No Q cells after 3 days in vitro with homeostatic cytokine IL-7, however in the presence of IL-2 or IL-2, TCR stimulation, and costimulation there was no deficit of DON pretreated cells (Figure 7k). These results suggest that pan-glutamine inhibition makes CD8 T cells more dependent on pro-stimulatory signals for survival and/or proliferation.

## Discussion

We found that glutamine inhibition strategies have distinct effects on CD8 T cell metabolism and activation. These results may have implications for glutamine-targeting therapies such as CB-839 and DON that are currently being developed as systemic agents or incorporated into ACT production strategies. Overall, our results are consistent with work in CD4 T cell differentiation which demonstrated distinct effects on Th1, Th17, and iTreg differentiation depending on different glutamine inhibition strategies (7–11, 14, 16). Although GLS-specific inhibition by CB-839 yielded smaller magnitude changes compared to DON and No Q, it was not simply a milder phenotype. Strikingly, CB-839 cells demonstrated a more glycolytic phenotype with reduced basal oxygen consumption compared to DON and No Q, suggesting that metabolic adaptations differ between GLS-specific and pan-glutamine inhibitory strategies. Conceptually, both DON and No Q globally block glutamine utilization, yet these treatments also yielded different phenotypes. DON has been shown to inhibit multiple glutamine-utilizing enzymes implicated across multiple metabolic processes, including glutaminase, glutamate synthase, asparagine synthetase, carbamyl phophate synthetase, NAD synthetase, and fructose-6-phosphate amidotransferase. (30). DON treatment dysregulated histone acetylation and methylation and had the most divergent transcriptional signature, whereas No Q cells upregulated autophagy transcripts and the utilization of other amino acids besides glutamine. DON and No Q cells also had marked differences *in vivo*, where DON-treated CD8 T cells did not expand or persist as well but had preserved memory proliferation on secondary antigen encounter, but No Q cells had reduced secondary response proliferation. These differences may be due to several factors. It is possible that the ability to synthesize and use low levels of glutamine in No Q cells permitted adaptation, whereas DON cells were prevented from utilizing glutamine for biological processes. This idea has been explored with glucose-restricted culture conditions to enhance anti-tumor T cell ACT (31). Alternatively, DON is an irreversible competitive inhibitor, so although cells were washed prior to adoptive transfer DON treatment may have directly impaired cells *in vivo* reducing their expansion and/or viability.

Our results suggest that DON pretreatment impairs the effectiveness of CD8 T cell adoptive therapy primarily by reducing the proliferation or persistence of antigen-specific cells. The timing of glutamine inhibition, therefore, may play an important role in cell outcomes. This stands in contrast to previous work that showed systemic DON treatment *in vivo* enhances CD8 function while weakening cancer cells (19) and that CD8 T cell ACT with DON pretreatment improves tumor control (17). *In vivo* treatment may differ from *in vitro* pretreatment of ACT by a lower tissue concentration of DON, DON affecting other cells in the TME (21), and treatment of CD8 T cells at later stages of activation and differentiation, not only the first 48hr of activation. It is also possible that there are optimal “goldilocks” ranges of glutamine concentration for different T cell subsets across inflammatory contexts.

Author Manuscript Author Manuscript Author Manuscript Author Manuscript

Consistent with this theory, targeted pharmacologic inhibition of glutamine uptake in cancer cells reduced “glutamine steal” by cancer cells from CD8 T cells, enhancing their cytotoxic activity (32). The previous study examining DON and No Q conditions for anti-tumor ACT measured phenotypes 96hr after activation, washed out treatments and replaced with control conditions for the final 24–48hr of activation, activated T cells with αCD3/28 antibodies instead of peptide, and used the EL4-OVA thymoma tumor model (17). These method differences may account for our different results and demonstrate how subtle changes in ACT manufacture or tumor types can lead to substantial differences in anti-tumor efficacy. It is possible that different levels of inhibition of GLS and other enzymes by 1μM CB-839 versus DON, or their off-target effects, may be contributing to the phenotypes measured here, although similar phenotypes with *Gls*-deficiency are support a specific effect of inhibition.

Multiple outstanding questions remain from this work. Targeted CRISPR screens focused on genes involved in glutamine transport and metabolism in conjunction with CB-839, DON, and No Q treatment may advance our understanding of how to best modulate glutamine metabolism for anti-tumor ACT (33). Here, DON treatment had marked effects on H3K27 acetylation and methylation, but it remains unclear to what extent glutamine’s downstream metabolite flux might directly regulate epigenetic changes, particularly early in T cell activation. DON treatment decreased both H3K27 methylation and acetylation with associated changes in gene transcripts, so it may be hypothesized that glutamine directly regulates these modifications. Finally, this work demonstrated the importance of investigating how therapeutics affect diverse cells in the tumor microenvironment depending on their own unique metabolic programs and functions (34).

## Supplementary Material

Refer to Web version on PubMed Central for supplementary material.

## Acknowledgements

We thank members of the Jeffrey and W. Kimryn Rathmell laboratories for their constructive input; Holly Algood, Meena Madhur, Michael Savona, and Young Kim for their comments; and the Justin Balko, Young Kim and Paula Hurley laboratories for the use of their tumor dissociators. The Vanderbilt VANTAGE Core provided technical assistance for this work. The NIH Tetramer facility provided SIINFEKL-specific tetramer.

**Funded by:**

F30 CA239367 (M.Z.M.), T32 GM007347 (M.Z.M., E.L.F., B.I.R.), F31 CA261049 (M.M.W.), K00 CA234920 (J.E.B.), F30 CA247202 (B.I.R.), CDA 5IK2BX004585 (R.T.O.), R01 CA217987 (J.C.R.), R01 DK105550 (J.C.R.). The VANTAGE core is supported in part by a CTSA Grant (5UL1 RR024975-03), the Vanderbilt Ingram Cancer Center (P30 CA68485), the Vanderbilt Vision Center (P30 EY08126) and the NIH/NCRR (G20 RR030956).

**Disclosures**

Dr. Jeffrey Rathmell is a founder, scientific advisory board member, and stockholder of Sitryx Therapeutics, a scientific advisory board member and stockholder of Caribou Biosciences, a member of the scientific advisory board of Nirogy Therapeutics, has consulted for Merck, Pfizer, and Mitobridge within the past three years, and has received research support from Incyte Corp., Calithera Biosciences, and Tempest Therapeutics.

Author Manuscript Author Manuscript Author Manuscript Author Manuscript

## References


1. Wise DR, and Thompson CB. 2010. Glutamine addiction: a new therapeutic target in cancer. Trends Biochem Sci 35: 427–433. [PubMed: 20570523]
2. Altman BJ, Stine ZE, and Dang C. v.. 2016. From Krebs to clinic: glutamine metabolism to cancer therapy. Nat Rev Cancer 16: 619–634. [PubMed: 27492215]
3. Lemberg KM, Gori SS, Tsukamoto T, Rais R, and Slusher BS. 2022. Clinical development of metabolic inhibitors for oncology. Journal of Clinical Investigation 132.
4. Lemberg KM, Vornov JJ, Rais R, and Slusher BS. 2018. We're Not "DON" Yet: Optimal Dosing and Prodrug Delivery of *6-Diazo-5-oxo-L-norleucine*. Mol Cancer Ther 17: 1824–1832. [PubMed: 30181331]
5. Kishton RJ, Sukumar M, and Restifo NP. 2017. Metabolic Regulation of T Cell Longevity and Function in Tumor Immunotherapy. Cell Metab 26: 94–109. [PubMed: 28683298]
6. Wang R, Dillon CP, Shi LZ, Milasta S, Carter R, Finkelstein D, McCormick LL, Fitzgerald P, Chi H, Munger J, and Green DR. 2011. The Transcription Factor Myc Controls Metabolic Reprogramming upon T Lymphocyte Activation. Immunity 35: 871–882. [PubMed: 22195744]
7. Carr EL, Kelman A, Wu GS, Gopaul R, Senkevitch E, Aghvanyan A, Turay AM, and Frauwirth KA. 2010. Glutamine Uptake and Metabolism Are Coordinately Regulated by ERK/MAPK during T Lymphocyte Activation. The Journal of Immunology 185: 1037–1044. [PubMed: 20554958]
8. Klysz D, Tai X, Robert PA, Craveiro M, Cretenet G, Oburoglu L, Mongellaz C, Floess S, Fritz V, Matias MI, Yong C, Surh N, Marie JC, Huehn J, Zimmermann V, Kinet S, Dardalhon V, and Taylor N. 2015. Glutamine-dependent α-ketoglutarate production regulates the balance between T helper 1 cell and regulatory T cell generation. Sci Signal 8.
9. Xu T, Stewart KM, Wang X, Liu K, Xie M, Ryu JK, Li K, Ma T, Wang H, Ni L, Zhu S, Cao N, Zhu D, Zhang Y, Akassoglou K, Dong C, Driggers EM, and Ding S. 2017. Metabolic control of TH17 and induced Treg cell balance by an epigenetic mechanism. Nature 548: 228–233. [PubMed: 28783731]
10. Nakaya M, Xiao Y, Zhou X, Chang J-H, Chang M, Cheng X, Blonska M, Lin X, and Sun S-C. 2014. Inflammatory T Cell Responses Rely on Amino Acid Transporter ASCT2 Facilitation of Glutamine Uptake and mTORC1 Kinase Activation. Immunity 40: 692–705. [PubMed: 24792914]
11. Xia X, Cao G, Sun G, Zhu L, Tian Y, Song Y, Guo C, Wang X, Zhong J, Zhou W, Li P, Zhang H, Hao J, Li Z, Deng L, Yin Z, and Gao Y. 2020. GLS1-mediated glutaminolysis unbridled by MALT1 protease promotes psoriasis pathogenesis. Journal of Clinical Investigation 130: 5180–5196. [PubMed: 32831293]
12. Kono M, Yoshida N, Maeda K, Suárez-Fueyo A, Kyttaris VC, and Tsokos GC. 2019. Glutaminase 1 Inhibition Reduces Glycolysis and Ameliorates Lupus-like Disease in MRL / *lpr* Mice and Experimental Autoimmune Encephalomyelitis. Arthritis & Rheumatology 71: 1869–1878. [PubMed: 31233276]
13. Kono M, Yoshida N, Maeda K, and Tsokos GC. 2018. Transcriptional factor ICER promotes glutaminolysis and the generation of Th17 cells. Proceedings of the National Academy of Sciences 115: 2478–2483.
14. Johnson MO, Wolf MM, Madden MZ, Andrejeva G, Sugiura A, Contreras DC, Maseda D, Liberti MV, Paz K, Kishton RJ, Johnson ME, de Cubas AA, Wu P, Li G, Zhang Y, Newcomb DC, Wells AD, Restifo NP, Rathmell WK, Locasale JW, Davila ML, Blazar BR, and Rathmell JC. 2018. Distinct Regulation of Th17 and Th1 Cell Differentiation by Glutaminase-Dependent Metabolism. Cell 175.
15. Chisolm DA, Savic D, Moore AJ, Ballesteros-Tato A, León B, Crossman DK, Murre C, Myers RM, and Weinmann AS. 2017. CCCTC-Binding Factor Translates Interleukin 2- and α-Ketoglutarate-Sensitive Metabolic Changes in T Cells into Context-Dependent Gene Programs. Immunity 47: 251–267.e7. [PubMed: 28813658]
16. Sinclair L. v, Rolf J, Emslie E, Shi Y-B, Taylor PM, and Cantrell DA. 2013. Control of amino-acid transport by antigen receptors coordinates the metabolic reprogramming essential for T cell differentiation. Nat Immunol 14: 500–508. [PubMed: 23525088]

Author Manuscript Author Manuscript Author Manuscript Author Manuscript

17. Nabe S, Yamada T, Suzuki J, Toriyama K, Yasuoka T, Kuwahara M, Shiraishi A, Takenaka K, Yasukawa M, and Yamashita M. 2018. Reinforce the antitumor activity of CD 8 $^{+}$ T cells via glutamine restriction. Cancer Sci 109: 3737–3750. [PubMed: 30302856]

18. Varghese S, Pramanik S, Williams LJ, Hodges HR, Hudgens CW, Fischer GM, Luo CK, Knighton B, Tan L, Lorenzi PL, Mackinnon AL, McQuade JL, Hailemichael Y, Roszik J, Peng W, and Vashisht Gopal YN. 2021. The Glutaminase Inhibitor CB-839 (Telaglenastat) Enhances the Antimelanoma Activity of T-Cell–Mediated Immunotherapies. Mol Cancer Ther 20: 500–511. [PubMed: 33361272]

19. Leone RD, Zhao L, Englert JM, Sun I-M, Oh M-H, Sun I-H, Arwood ML, Bettencourt IA, Patel CH, Wen J, Tam A, Blosser RL, Prchalova E, Alt J, Rais R, Slusher BS, and Powell JD. 2019. Glutamine blockade induces divergent metabolic programs to overcome tumor immune evasion. Science (1979) 366: 1013–1021.

20. Huang M, Xiong D, Pan J, Zhang Q, Sei S, Shoemaker RH, Lubet RA, Montuenga LM, Wang Y, Slusher BS, and You M. 2022. Targeting Glutamine Metabolism to Enhance Immunoprevention of EGFR-Driven Lung Cancer. Advanced Science 2105885.

21. Oh M-H, Sun I-H, Zhao L, Leone RD, Sun I-M, Xu W, Collins SL, Tam AJ, Blosser RL, Patel CH, Englert JM, Arwood ML, Wen J, Chan-Li Y, Tenora L, Majer P, Rais R, Slusher BS, Horton MR, and Powell JD. 2020. Targeting glutamine metabolism enhances tumor-specific immunity by modulating suppressive myeloid cells. Journal of Clinical Investigation 130: 3865–3884. [PubMed: 32324593]

22. Best SA, Gubser PM, Sethumadhavan S, Kersbergen A, Negrón Abril YL, Goldford J, Sellers K, Abeysekera W, Garnham AL, McDonald JA, Weeden CE, Anderson D, Pirman D, Roddy TP, Creek DJ, Kallies A, Kingsbury G, and Sutherland KD. 2022. Glutaminase inhibition impairs CD8 T cell activation in STK11-/Lkb1-deficient lung cancer. Cell Metab 34: 874–887.e6. [PubMed: 35504291]

23. Ahluwalia GS, Grem JL, Hao Z, and Cooney DA. 1990. Metabolism and action of amino acid analog anti-cancer agents. Pharmacol Ther 46: 243–271. [PubMed: 2108451]

24. O'Neil RT, Saha S, Veach RA, Welch RC, Woodard LE, Rooney CM, and Wilson MH. 2018. Transposon-modified antigen-specific T lymphocytes for sustained therapeutic protein delivery in vivo. Nat Commun 9: 1325. [PubMed: 29636469]

25. Brockstedt DG, Giedlin MA, Leong ML, Bahjat KS, Gao Y, Luckett W, Liu W, Cook DN, Portnoy DA, and Dubensky TW. 2004. *Listeria* -based cancer vaccines that segregate immunogenicity from toxicity. Proceedings of the National Academy of Sciences 101: 13832–13837.

26. Govindaraju V, Young K, and Maudsley AA. 2000. Proton NMR chemical shifts and coupling constants for brain metabolites. NMR Biomed 13: 129–153. [PubMed: 10861994]

27. Skene PJ, and Henikoff S. 2017. An efficient targeted nuclease strategy for high-resolution mapping of DNA binding sites. Elife 6.

28. Sukumar M, Liu J, Mehta GU, Patel SJ, Roychoudhuri R, Crompton JG, Klebanoff CA, Ji Y, Li P, Yu Z, Whitehill GD, Clever D, Eil RL, Palmer DC, Mitra S, Rao M, Keyvanfar K, Schrump DS, Wang E, Marincola FM, Gattinoni L, Leonard WJ, Muranski P, Finkel T, and Restifo NP. 2016. Mitochondrial Membrane Potential Identifies Cells with Enhanced Stemness for Cellular Therapy. Cell Metab 23: 63–76. [PubMed: 26674251]

29. Britt EC, v John S, Locasale JW, and Fan J. 2020. Metabolic regulation of epigenetic remodeling in immune cells. Curr Opin Biotechnol 63: 111–117. [PubMed: 31954223]

30. Pinkus LM 1977. [45] Glutamine binding sites. In 414–427.

31. Klein Geltink RI, Edwards-Hicks J, Apostolova P, O'Sullivan D, Sanin DE, Patterson AE, Puleston DJ, Ligthart NAM, Buescher JM, Grzes KM, Kabat AM, Stanczak M, Curtis JD, Hässler F, Uhl FM, Fabri M, Zeiser R, Pearce EJ, and Pearce EL. 2020. Metabolic conditioning of CD8+ effector T cells for adoptive cell therapy. Nat Metab 2: 703–716. [PubMed: 32747793]

32. Edwards DN, Ngwa VM, Raybuck AL, Wang S, Hwang Y, Kim LC, Cho SH, Paik Y, Wang Q, Zhang S, Manning HC, Rathmell JC, Cook RS, Boothby MR, and Chen J. 2021. Selective glutamine metabolism inhibition in tumor cells improves antitumor T lymphocyte activity in triple-negative breast cancer. Journal of Clinical Investigation 131.

Author Manuscript Author Manuscript Author Manuscript Author Manuscript

33. Sugiura A, Andrejeva G, Voss K, Heintzman DR, Xu X, Madden MZ, Ye X, Beier KL, Chowdhury NU, Wolf MM, Young AC, Greenwood DL, Sewell AE, Shahi SK, Freedman SN, Cameron AM, Foerch P, Bourne T, Garcia-Canaveras JC, Karijolich J, Newcomb DC, Mangalam AK, Rabinowitz JD, and Rathmell JC. 2022. MTHFD2 is a metabolic checkpoint controlling effector and regulatory T cell fate and function. Immunity 55.

34. Reinfeld BI, Madden MZ, Wolf MM, Chytil A, Bader JE, Patterson AR, Sugiura A, Cohen AS, Ali A, Do BT, Muir A, Lewis CA, Hongo RA, Young KL, Brown RE, Todd VM, Huffstater T, Abraham A, O'Neil RT, Wilson MH, Xin F, Tantawy MN, Merryman WD, Johnson RW, Williams CS, Mason EF, Mason FM, Beckermann KE, vander Heiden MG, Manning HC, Rathmell JC, and Rathmell WK. 2021. Cell-programmed nutrient partitioning in the tumour microenvironment. Nature 593.

Author Manuscript Author Manuscript Author Manuscript Author Manuscript

**Key points**

Distinct glutamine inhibition strategies cause unique changes to CD8 T cell function

T cell metabolism compensates according to how glutamine metabolism is targeted

Timing and strategy for use of glutamine-targeting agents modify T cell outcomes

Author Manuscript
Author Manuscript
Author Manuscript
Author Manuscript



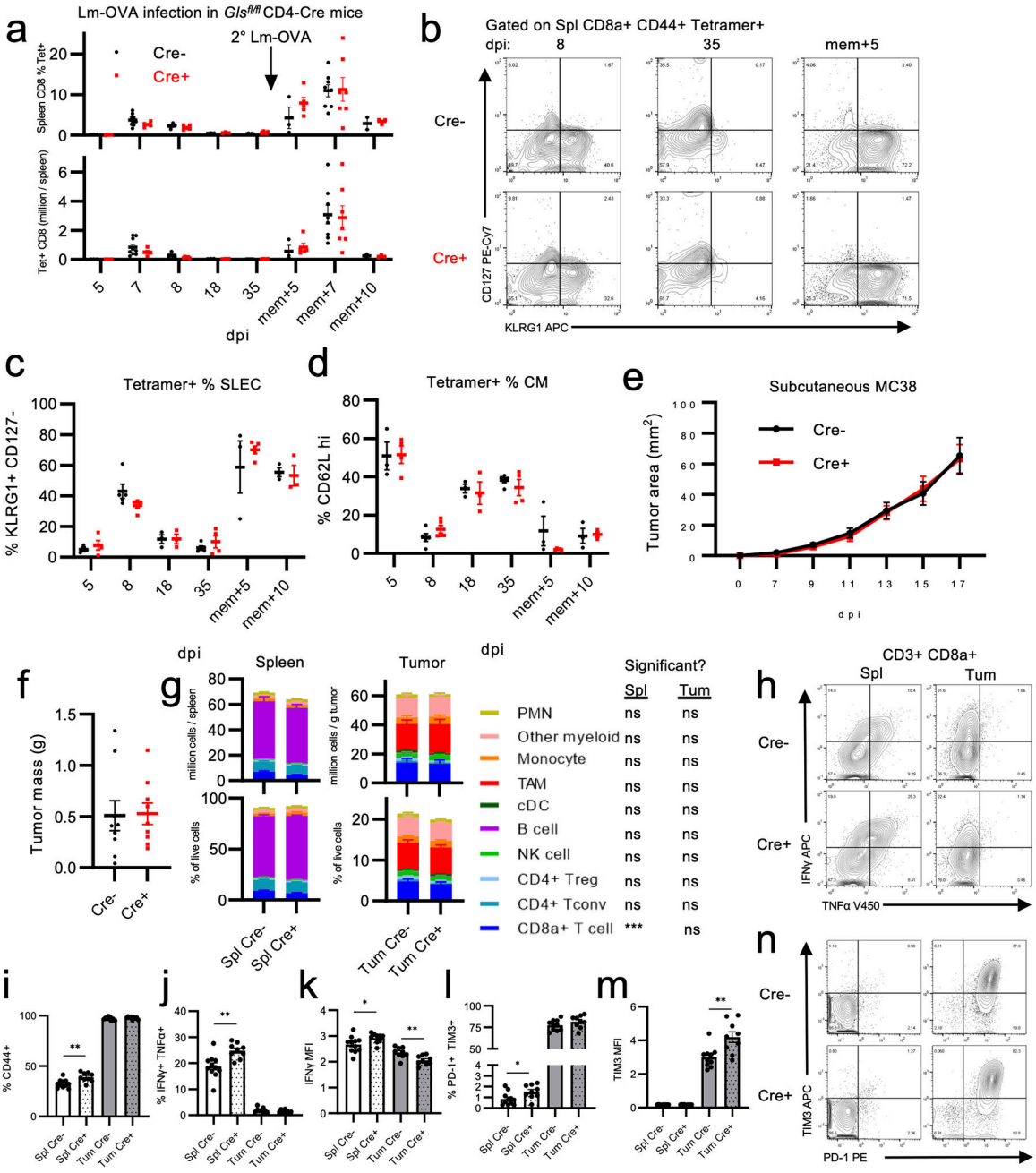


**Figure 1: *Gls* deficiency in T cells does not affect responses to acute infection or tumors**

**a**, Spleen (Spl) Lm-OVA antigen-specific tetramer$^{+}$ CD8 T cells as % of total CD8 T cells (top) and total number per spleen (bottom) in CD4-Cre$^{-}$ control or CD4-Cre$^{+}$ knockout *Gls*$^{fl/fl}$ mice at indicated days post infection (dpi) or after memory response to secondary Lm-OVA infection >35 days post initial infection (mem). **b-d**, Short-lived effector cell (SLEC) (**b,c**) and central memory (CM) (**d**) phenotypes of tetramer$^{+}$ CD8 T cells after Lm-OVA. **e-f**, Growth curve (**e**) and final tumor mass (**f**) of subcutaneous MC38 tumors in CD4-Cre$^{-}$ control or CD4-Cre$^{+}$ knockout *Gls*$^{fl/fl}$ mice. **g**, Immune cell abundance (top row) and proportion (bottom row) in spleens and MC38 tumors (Tum) and significance

Author Manuscript Author Manuscript Author Manuscript Author Manuscript

between genotypes. **h-n**, Phenotype of spleen and tumor CD8 T cells by genotype showing intracellular cytokine production (**h, j-k**), CD44 (**i**), and coinhibitory markers (**l-n**). Panels (a-d) show pooled results from 2 independent experiments (n=3–8 mice per timepoint per genotype). Panels (e-n) show the results of a representative experiment of 2 independent experiments (n=9–11 mice). Each data point represents a biological replicate and error bars show SEM. Each comparison and timepoint was compared by Welch's 2-tailed t-test ($p>0.05$ Not significant [ns] or no asterisk, * $p<0.05$, ** $p<0.01$, *** $p<0.001$). See Supplemental Figure 1 for flow cytometry gating schemes.

Author Manuscript Author Manuscript Author Manuscript Author Manuscript

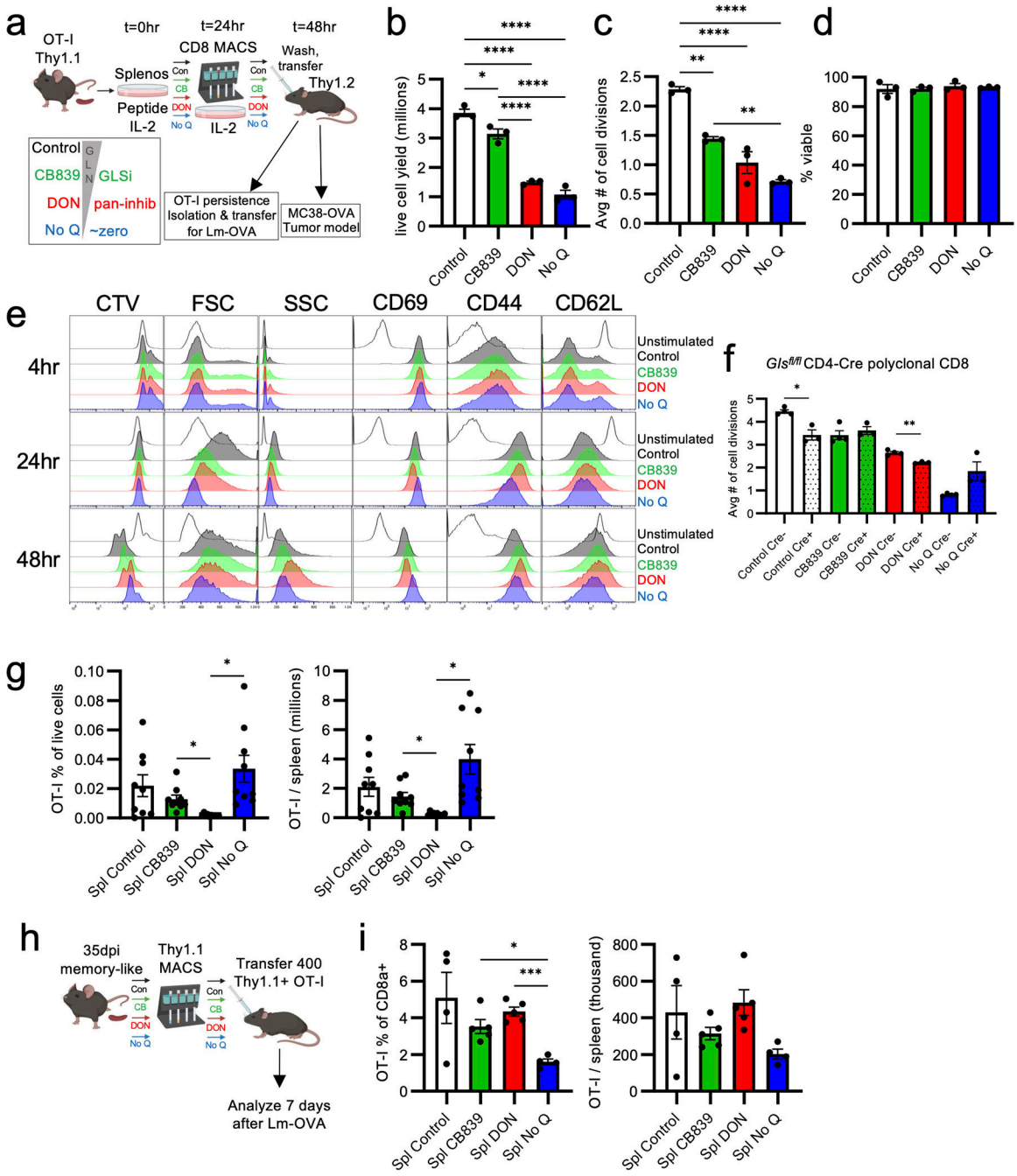


**Figure 2: Glutamine inhibition strategies induce differences in CD8 T cell memory responses**

**a**, Experimental scheme of *in vitro* OT-I CD8 T cell activation and culture before adoptive transfer. **b-d**, Live cell yield determined by automated trypan count (**b**), average number of cell divisions determined by CellTrace Violet (CTV) dilution (**c**), and viability determined by automated trypan count (**d**) of OT-I CD8 T cells at 48hr post-activation (n=3 mice). **e**, Proliferation (CTV), size (forward scatter, FSC), granularity (side scatter, SSC), and activation markers of OT-I CD8 T cells at indicated timepoints in different glutamine treatments. **f**, Average number of cell divisions determined by CTV dilution of CD4-Cre$^{-}$

Author Manuscript Author Manuscript Author Manuscript Author Manuscript

control or CD4-Cre$^{+}$ knockout *Gls*$^{fl/fl}$ CD8 T cells in different glutamine treatments (n=3–4 mice). **g**, Abundance of persisting Thy1.1$^{+}$ OT-I CD8 T cells 35 days after adoptive transfer in the spleens (Spl) of naïve Thy1.2$^{+}$ mice (n=9–10 mice). **h**, Experimental scheme for isolation of previously glutamine-treated Thy1.1$^{+}$ OT-I CD8 T cells, transfer into naïve Thy1.2$^{+}$ mice, and infection with Lm-OVA. **i**, Abundance of splenic secondary effector Thy1.1$^{+}$ OT-I CD8 T cells 7 days after Lm-OVA infection. Panels (b-e) show representative results from >5 independent experiments. Panel (f) shows representative results of one of 2 independent experiments. Panel (g) shows pooled results from 2 independent experiments. Each data point represents a biological replicate and error bars show SEM. Asterisks indicate p-values of Welch's 2-tailed t-test (f) or Brown-Forsythe and Welch ANOVA tests with multiple comparisons (b-d, g, i) (* $p<0.05$, ** $p<0.01$, *** $p<0.001$, **** $p<0.0001$).

Author Manuscript Author Manuscript Author Manuscript Author Manuscript

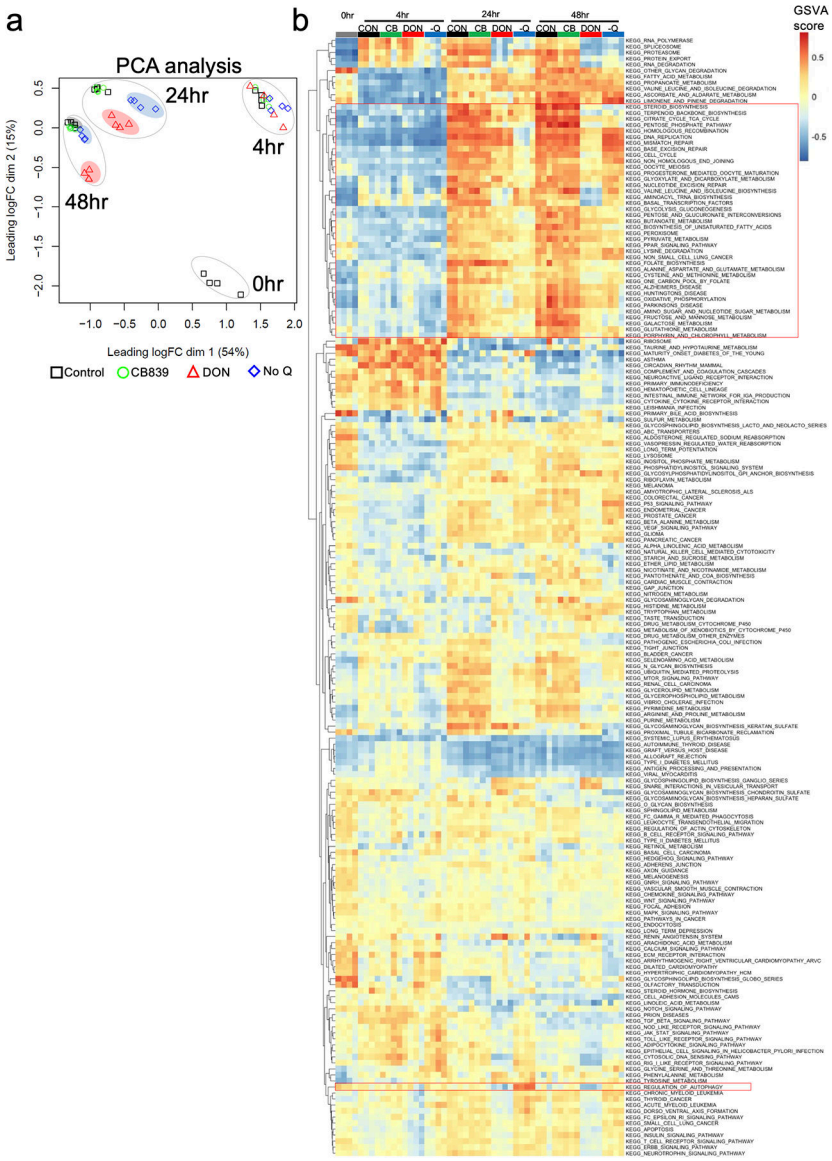


**Figure 3: Transcriptional signatures of glutamine-inhibited CD8 T cells**

**a-b**, Principal Component Analysis (PCA) (**a**) and heatmap of KEGG gene set variation analysis (GSVA) scores (**b**) of RNAseq transcriptomes from CD8 T cells at indicated timepoints and with glutamine treatments. Red boxes highlight pathway clusters of anabolic and cell cycle-related gene sets (top) and autophagy (bottom). Analysis from n=4 biological replicates.

Author Manuscript
Author Manuscript
Author Manuscript
Author Manuscript



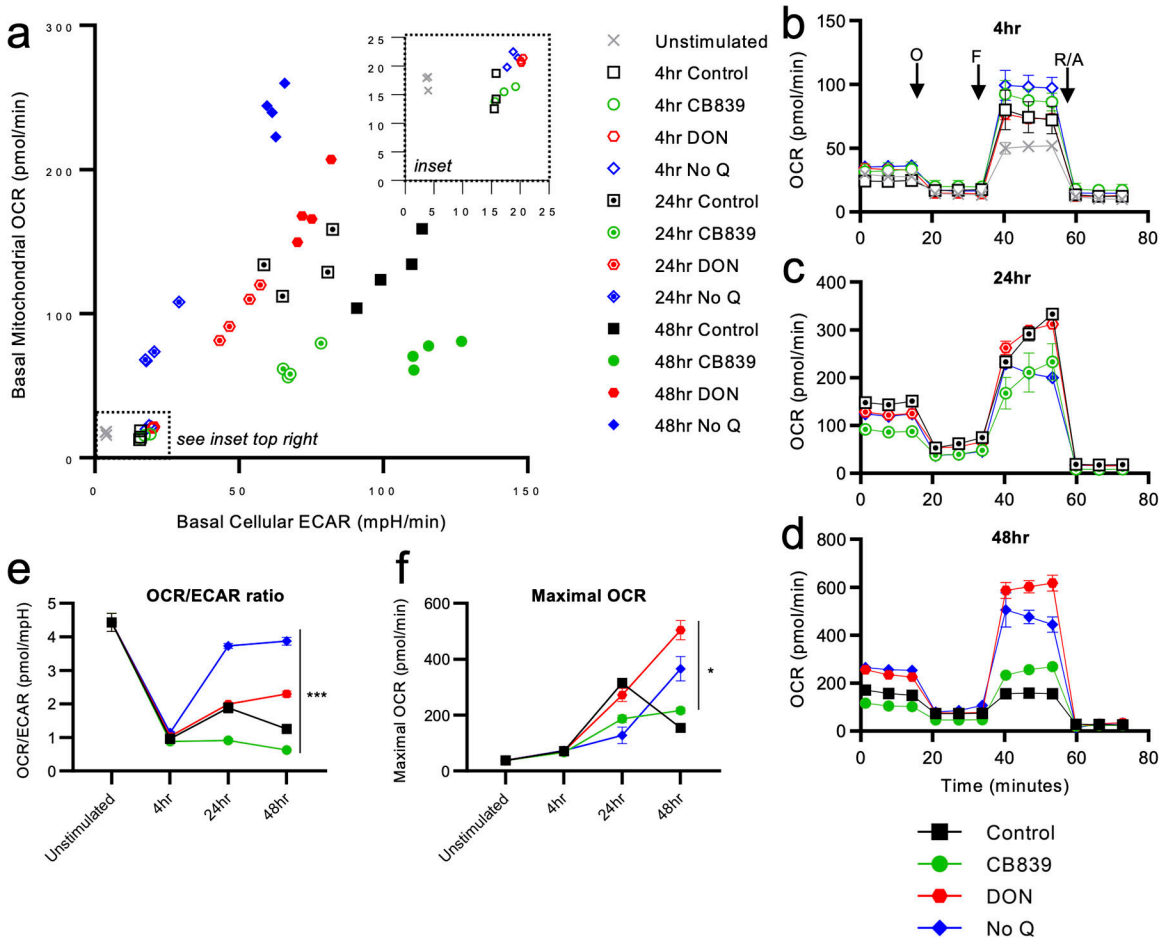


**Figure 4: Glutamine inhibition strategies cause divergent metabolic differentiation**

Extracellular flux analysis was performed on OT-I CD8 T cells at indicated timepoints of differentiation with different glutamine inhibition strategies (n=3–4 mice). **a**, Basal mitochondrial oxygen consumption rate (OCR) versus basal cellular extracellular acidification rate (ECAR). 0hr and 4hr timepoints are expanded in upper right inset. **b-d**, Representative OCR tracings of Mitostress tests for a biological replicate (n>2 technical replicates per biological replicate) after sequential injections of oligomycin, FCCP, and rotenone/antimycin A. **e-f**, Basal OCR/ECAR ratio (**e**) and maximal OCR (**f**) over time from indicated timepoints and glutamine conditions. Asterisks indicate all 2-way comparisons $p<0.001$ (e) and all comparisons except control vs. CB-839 $p<0.05$ (f). Each data point represents a biological replicate and error bars show SEM. Data are representative of at least 2 independent experiments.

Author Manuscript
Author Manuscript
Author Manuscript
Author Manuscript



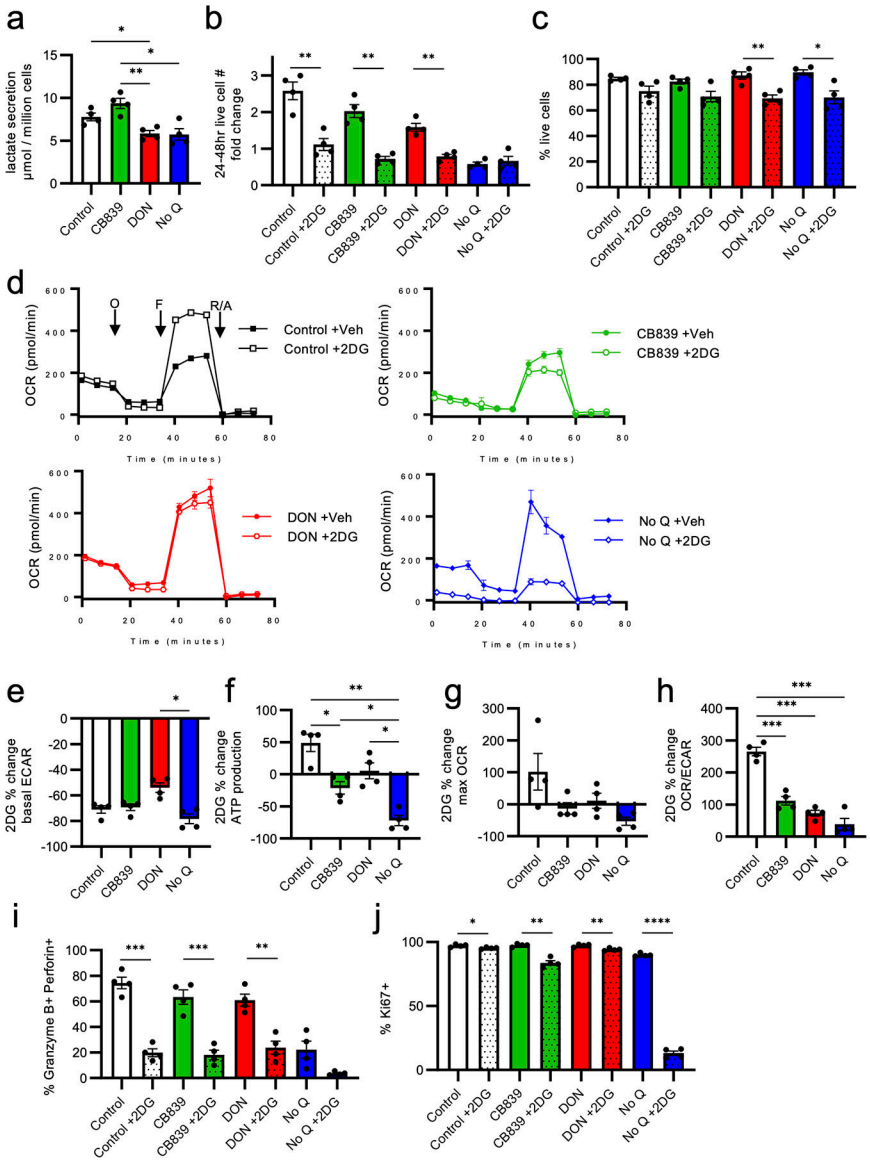


**Figure 5: Glutamine inhibition increases glucose dependency**

**a**, Net cellular lactate secretion of glutamine-treated OT-I CD8 T cells from 24–48hr in culture (n=4 mice). **b-c**, Live cell yield (**b**) and viability (**c**) of. **d**, Representative oxygen consumption rate (OCR) tracings of Mitostress tests (n>2 technical replicates per biological replicate) after sequential injections of oligomycin, FCCP, and rotenone/antimycin A of OT-I CD8 T cells at 48hr after glutamine treatments with and without 2-deoxyglucose (2DG). **e-h**, Percent change from vehicle treated to 2DG treated cells of basal ECAR (**e**), OCR ATP production (**f**), maximal OCR (**g**), and the basal OCR/ECAR ratio (**h**) for OT-I CD8 T cells at 48hr (n=4 mice). **i-l**, Flow cytometry measurement of CD69 MFI (**i**), CD25 MFI (**j**), % Granzyme $B^+$ $Perforin^+$ (**k**), and % $Ki67^+$ (**l**) in OT-I CD8 T cells with indicated treatments at 48hr (n=4 mice). Each data point represents a biological replicate (n=3–4 mice) and error bars show SEM. Data are representative of 2 independent experiments. Asterisks indicate

p-values of Welch's 2-tailed t-test (b-c, i-j) or Brown-Forsythe and Welch ANOVA tests with multiple comparisons (a, e-h) (* $p<0.05$, ** $p<0.01$, *** $p<0.001$, **** $p<0.0001$).

Author Manuscript Author Manuscript Author Manuscript Author Manuscript

Author Manuscript Author Manuscript Author Manuscript Author Manuscript

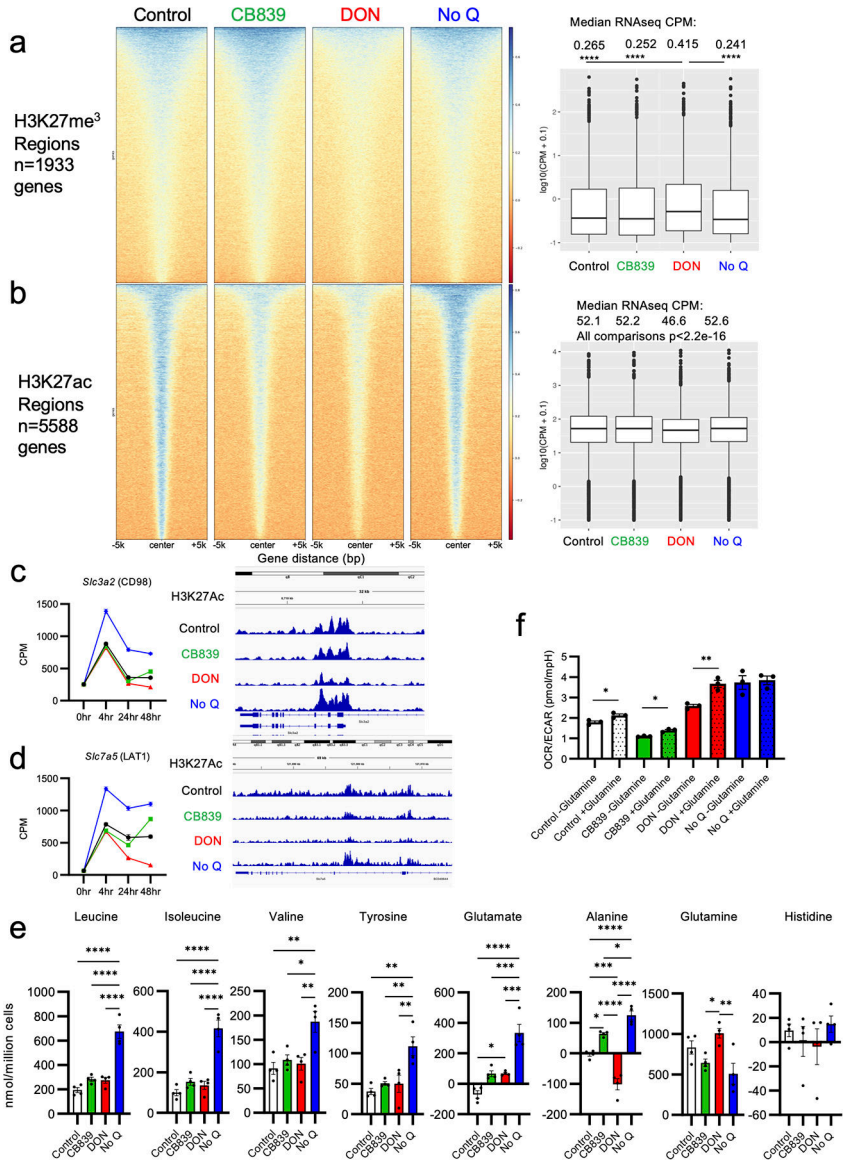


**Figure 6: Glutamine inhibition alters H3K27 PTMs associated with metabolic adaptation.**

**a-b**, H3K27me$^3$ (**a**) and H3K27Ac (**b**) levels around identified peaks (left) and RNAseq transcript counts per million (CPM) for genes with promoters detected from respective CUT&RUN peaks (right) from OT-I CD8 T cells at 48hr. Data are the mean of n=2 mice. **c-d**, *Slc3a2* (**c**) and *Slc7a5* (**d**) transcript levels (CPM) at different timepoints (left, n=4 mice) and H3K27Ac level around promoters at 48hr (left, average of n=2 mice). **e**, Net cellular uptake (positive value) and secretion (negative value) of indicated amino acids in OT-I CD8 T cells from 24 to 48hr in culture (n=4 mice). **f**, OCR/ECAR ratios of indicated pretreated OT-I CD8 T cells at 48hr with or without glutamine added to extracellular flux media (n=3 mice). Metabolism data are representative of 2 independent experiments. Asterisks indicate p-values of Wilcoxon test (a-b), Welch's 2-tailed t-test (f), or Brown-Forsythe and Welch ANOVA tests with multiple comparisons (e) (* $p<0.05$, ** $p<0.01$, *** $p<0.001$, **** $p<0.0001$).

Author Manuscript Author Manuscript Author Manuscript Author Manuscript

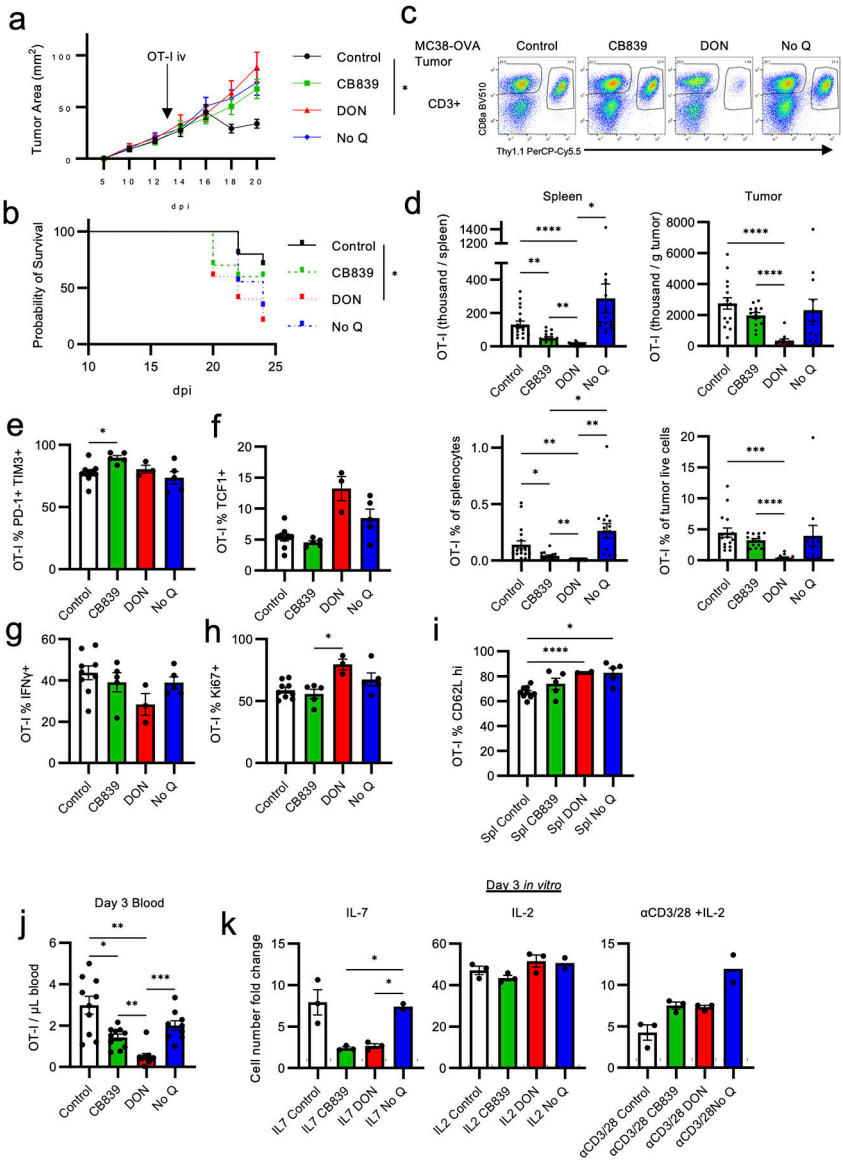


**Figure 7: Glutamine inhibition strategies cause divergent effects on anti-tumor ACT.**

**a-b**, MC38-OVA tumor growth (**a**) and mouse survival (**b**) after treatment on day 13 (arrow) with 500,000 pretreated OT-I CD8 T cells. **c**, Representative flow cytometry plots of tumor-infiltrating Thy1.1$^{+}$ OT-I cell abundance. **d**, Quantification of OT-I cell abundance in spleens and MC38-OVA tumors. **e-h**, Flow cytometry quantification of tumor-infiltrating OT-I cells for % PD-1$^{+}$ TIM3$^{+}$ (**e**), % TCF1$^{+}$ (**f**), % IFN$\gamma^{+}$ following *ex vivo* PMA/ionomycin stimulation (**g**), and % Ki67$^{+}$ (**h**). **i**, Flow cytometry quantification of splenic OT-I T cell % CD62L$^{hi}$. **j**, Quantification of adoptively transferred pretreated OT-I cells in murine peripheral blood 3 days after adoptive transfer. **k**, Fold increase in pretreated OT-I cell number after 3 additional days of culture in control media with indicated stimulation conditions. Each dot represents a biological replicate and error bars show SEM. Data are representative of at least 2 independent experiments (**a-c**, **e-k**) or merged from 3 independent experiments (n=11–16 mice) (**d**). In **a**, asterisk shows significance between

Author Manuscript Author Manuscript Author Manuscript Author Manuscript

control and DON groups at day 20. In **b**, asterisk indicates significance between control and DON survival curves according to Log-rank (Mantel-Cox) test (n=10 except for n=9 for No Q group). Unless otherwise stated, asterisks indicate p-values of Brown-Forsythe and Welch ANOVA tests with multiple comparisons (* $p<0.05$, ** $p<0.01$, *** $p<0.001$, **** $p<0.0001$).